SEMI-ANNUAL REPORT

(for January - July 1995)

Contract Number NAS5-31363

OCEAN OBSERVATIONS WITH EOS/MODIS:

Algorithm Development and Post Launch Studies

Howard R. Gordon
University of Miami
Department of Physics
Coral Gables, FL 33124

(Submitted July 15, 1995)

MODIS Semi-Annual Report (1 January – 30 June 1995) contract NAS5–31363

Abstract

Several significant accomplishments were made during the present reporting period.

. An investigation of the influence of stratospheric aerosol on the performance of the atmospheric correction algorithm was carried out. The results indicate how the performance of the algorithm is degraded if the stratospheric aerosol is ignored. Use of the MODIS 1380 nm band to effect a correction for stratospheric aerosols was also studied. Simple algorithms such a subtracting the reflectance at 1380 run from the visible and near infrared bands do not significantly reduce the error. The ornly way found to significantly reduce their effects requires full knowledge of the stratospheric aerosol optical properties, and extensive radiative transfer computations for implementation.

- The development of a multi-layer Monte Carlo radiative transfer code that includes polarization by molecular and aerosol scattering and wind-induced sea surface roughness has been completed. Comparison tests with an existing two-layer successive order of scattering code suggests that both codes are capable of producing top-of-atmosphere radiances with errors usually < 0.1%. This code will be used to generate realistic pseudo data with which to test the atmospheric correction algorithm.

- An initial set of simulations to study the effects of ignoring the polarization of the ocean-atmosphere light field, in both the development of the atmospheric correction algorithm and the generation of the lookup tables used for operation of the algorithm, have been completed. The results suggest two important conclusions: (1) that most of the error due to the neglect of polarization can be removed by computing the Rayleigh contribution to the total reflectance using vector radiative transfer theory; and (2) the residual error in the water-leaving reflectance due to the neglect of polarization in constructing the lookup tables is usually ~ 0.001, and appears to vary in a systematic manner with viewing geometry.

- An algorithm was developed that can be used to invert the radiance exiting the top and bottom of the atmosphere to yield the columnar optical properties of the atmospheric aerosol under clear sky conditions over the oceans, for aerosol optical thicknesses as large as 2. The algorithm is capable of retrievals with such large optical thicknesses because all significant orders of multiple scattering are included. Combining an algorithm of this type with surface-based and high altitude aircraft-based radiance measurements could be useful for studying aerosol columnar optical properties over oceans and large lakes.

1. Atmospheric Correction Algorithm Development

a. Task Objectives:

During CY 1995 there are five objectives under this task:

(i) Investigate the effects of stratospheric aerosol and/or cirrus clouds on the performance of the proposed atmospheric correction algorithm.

(ii) Complete a multilayer Monte Carlo simulation code that includes the effects of aerosol and molecular scattering polarization (a vector radiative transfer code) and sea surface roughness.

(iii) Investigate the effects of ignoring the polarization of the atmospheric Light field on the performance of the proposed atmospheric correction algorithm.

(iv) Investigate the effects of vertical structure in the aerosol concentration and type on the behavior of the proposed atmospheric correction algorithm,

(v) Begin a detailed investigation of the performance of the correction algorithm in atmospheres with strongly absorbing aerosols.

b. Work Accomplished:

(i) We have completed the computations regarding the influence of stratospheric aerosols on atmospheric correction, and the possibility of using the 1380 nm MODIS band for removing their effects. A report covering the present status of this work is attached as Appendix 1

(ii) We have completed development and validation of a multilayer Monte Carlo code radiative transfer code to provide test pseudo data for examination of the performance of the proposed atmospheric correction algorithm in more realistic situations. The code solves the vector radiative transfer equation (i.e., it includes the effects of polarization) for the Stokes vector of the radiance exiting the top of the atmosphere. It also includes a wind-roughened sea surface at the lower boundary of the atmosphere. The atmosphere is divided into four broad regions: (1) the marine

boundary layer from the surface to 2 km, where the aerosol concentration is independent of altitude; (2) the free troposphere, where the aerosol concentrations varies in proportion to exp[-z/h], where z is the altitude (2-12 km) and *h* (the scale height) is 2 km; (3) the background stratosphere (12-30 km), where the aerosol concentration is also exponential with a scale height of 5 km; and (4) a volcanic region (20-25 km) within the stratosphere which can contain a uniformly mixed volcanic aerosol. The optical properties of each of the four regions can be characterized by indvidual aerosol models, and any of the regions can be free of aerosols if desired. Alternatively, the user can supply *any* vertical structure desired for the aerosol; however, no more than four different aerosol models *can* be used in a single simulation.

The final code was validated by comparison with an existing two-layer code[1] which employs the successive order of scattering method.[2] The aerosol model used in the code validation was that originally used by Gordon and Wang[3] and is similar to that used by Quenzel and Kastner[4] to represent a marine aerosol at 70% relative humidity. The size distribution was

$$\begin{aligned} \frac{dN}{dD} &= K, & D_0 < D \le D_1, \\ &= K\left(\frac{D_1}{D}\right)^{\nu+1}, & D_1 < D \le D_2, \\ &= 0, & D > D_2, \end{aligned}$$

with ν = 2.95, D_0 = 0.2 µm, D_1 = 0.4 µm, and D_2 = 17.5 µm, and the refractive index was 1.45 – 0.02i. The resulting, nonzero, elements of the scattering phase matrix are provided in Figure

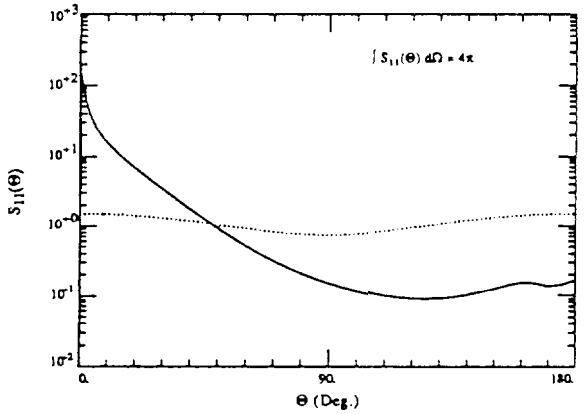

Figure 1a. S_{11} element of the scattering matrix for aerosols (solid line) and molecules (dotted line) as a function of the scattering angle. Note, $S_{22} = S_{11}$.

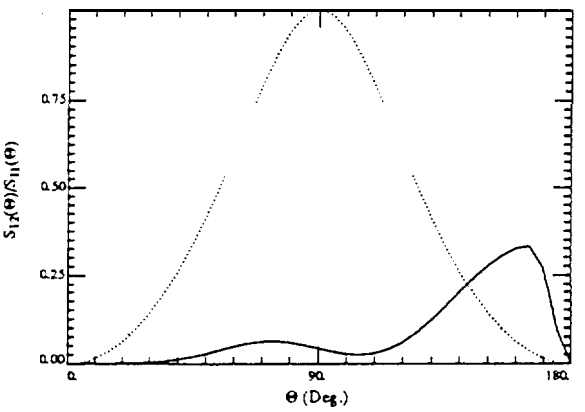

Figure 1b. S_{12} element of the scattering matrix for aerosols (solid line) and $-S_{12}$ for molecules (dotted line) as a function of the scattering angle. Note, $S_{21} = S_{12}$.

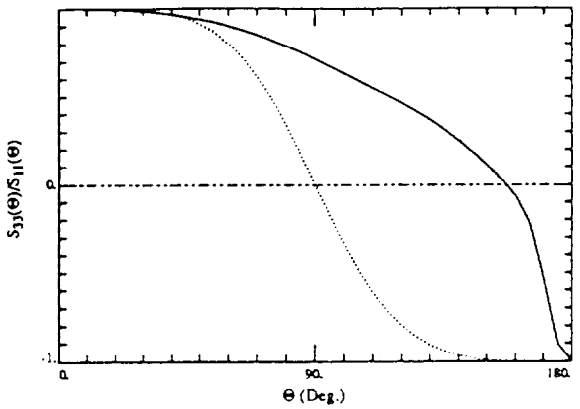

Figure 1c. S_{33} element of the scattering matrix for aerosols (solid line) and molecules (dotted line) as a function of the scattering angle. Note, $S_{44} = S_{33}$.

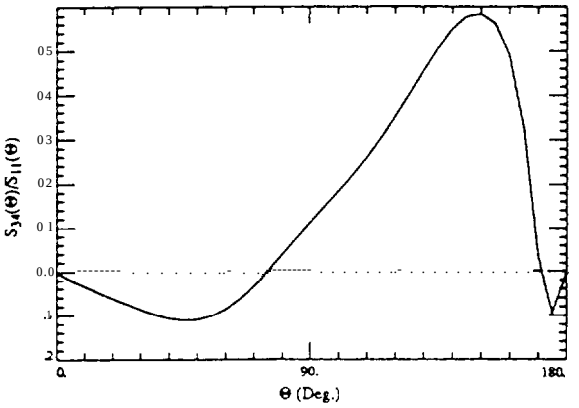

Figure 1d. S_{34} element of the scattering matrix for aerosols (solid line) and molecules ($S_{34} = 0$) as a function of the scattering angle. Note, $S_{43} = -S_{34}$.

1 along with those for Rayleigh scattering.

Samples of the differences between the two codes are provided in Tables 1 and 2. In the tables, "FMC" stands for Forward Monte Carlo, "SOM" for Successive Order Method, and "10^7 Diff" is the % difference between the two [l00*(FMC-SOM)/SOM] when 10 million photon histories are followed, while for "10^8 Diff" 100 million are followed. The Rayleigh and aerosol optical thickness are $T_r = 0.1$ and $T_a = 0.2$, respectively. The aerosol and molecules are uniformly mixed in a single layer. The single scattering albedo is 1 (no absorption). The solar zenith angle 80 is 60°, and three viewing directions (specified by the polar and azimuth angles and are examined:

View 1: = 2.28°, = 180°

View 2: = 39.88°, = 90°

View 3: = 60.15°, = 0°

For the rough ocean surface cases, the Cox-Munk surface slope standard deviation[5] = 0.2, which corresponds to a wind speed of approximately 7.5 m/s. Unidirectional wave shadowing[1,3] of one wave by another is utilized in the *incident* direction only.

In Table 1 we present the results for the case of a flat sea surface. They indicate that for view 1 and view 2 the difference in the two codes for the computed Stokes vector is $\leq$ 0.l%. The result for view 3 is very poor; however, this is due entirely to the fact that an insufficient number of Fourier orders (16) in the azimuthal decomposition of the radiance was used in the SOM computation. This leads to a significant error in the computed radiance when = because the radiance distribution exiting the top of the atmosphere has a sharp maximum near the specular image of the sun. This results from small-angle forward scattering by the aerosol followed or preceeded by reflection from the sea surface. A significantly larger number of Fourier orders would be required to accurately predict the radiance in this geometry using the SOM. If the aerosol is removed and a pure molecular-scattering atmosphere is considered, this large difference disappears and the error is comparable to that at for the other two views. We believe that in this geometry the radiance predicted by the Monte Carlo is far more accurate, as it does not suffer the need for Fourier decomposition. For $\phi = 0$ (views 1 and 3) a rough estimate of the Monte Carlo statistical fluctuation can be ascertained by the magnitude of the component U which must be identically zero in this geometry. For view 1, this is ~ 10^{-4} of I, which is consistent with an error of the order of 0.01% in I.

Table 2 provides the differences between the two codes in the case of a wind roughened sea surface. The differences for 10^{7} photon histories are now larger than in Table 1; however, increasing to 10^{8} photon histories significantly improves the agreement between the two codes. Note that in this case the anomalous error seen in Table 1 for view 3 is absent. The radiance is now a smoother function of direction near the specular image of the sun than for a flat ocean, and thus, fewer Fourier orders are required to accurately compute the radiation field. The computations provided *do not* contain the contribution due to direct sun glitter, i.e., the contribution from photons that reflect off the sea surface *without* interacting with the atmosphere. This component is absent in the Monte Carlo because the first collision is forced in the medium to reduce the statistical fluctuations. In the SOM, this component is removed from the computation because it would require using an enormous number of Fourier orders,[1] This is no blemish, however, since the direct sun glitter can be computed *exactly* in a very simple manner given the surface slope statistics. Thus, for the results in the tables, sky *glitter* is *included,* but if direct sun glitter is desired it must be computed separately

and added to the radiances provided by the code. Finally, it is important to note that to provide the best possible simulation of the rough surface effects, the Monte Carlo code treats multiple scattering by the sea surface, while the SOM code does not. Because of this, perfect agreement for the rough sea surface case is not possible.

We believe the results provided in the test above validates that both codes are capable of computing vector radiances with errors less than ~ 0.l% in the I component (unless is close to θ_0 for the SOM code). The Monte Carlo code will be used to study the performance of the atmospheric correction algorithm under more realistic conditions – a vertically stratified aerosol (type and concentration), a rough sea surface, and test pseudo data generated with full consideration of polarization of the light field.

(iii) Using the Monte Carlo simulation code described above, we have started a study of the error in the atmospheric correction algorithm caused by ignoring polarization. That is, as described in our ATBD for Normalized Water-leaving Radiance, the atmospheric correction algorithm uses a set of lookup tables relating the radiance produced by all photons interacting with the aerosol and those interacting with *both* aerosols and air molecules (Rayleigh scattering) to the radiance that would be observed from the aerosol alone were the radiative transfer process governed by single scattering. These lookup tables were generated for a set of candidate aerosol models and are based on ~ 33,000 separate radiative transfer simulations (including all orders of multiple scattering). Their generation, therefore involved a considerable investment in computational resources. To keep the table-generation time to a minimum, the approximation of scalar radiative transfer theory (polarization ignored) was employed. Thus, we need to understand the influence of this approximation on the correction algorithm. To effect this, we simply use our newly-developed Monte Carlo code to simulate the radiance under exact vector radiative transfer theory (effects of polarization on the transfer process are considered). Here, we report the results of the initial studies to assess the error in the algorithm caused by generating the lookup tables using scalar transfer theory.

In the initial studies, two comparisons are carried out. The Monte Carlo code is set to operate in a two-layer mode, with aerosols in the lower layer and all of the Rayleigh scattering confined to the upper layer. The sea surface is assumed to be flat (no wind). Thus the aerosol structure of

Table 1a: Comparison of Stokes Vector Calculations

Flat Ocean Surface; View 1

	I	Q	U	V
FMC	0.11569E-01	–0.46231E-02	0.91547E-06	0.19360E-06
SOM	0.11580E-01	–0.46257E-02	0.82666E-09	–.16649E-12
10^7 Diff(%)	0.02	-0.06	– – –	– – –

Table 1b: Comparison of Stokes Vector Calculations

Flat Ocean Surface ; View 2

	I	Q	U	V
FMC	0.14445E-01	0.50866E-02	-0.40972E-02	0.86810E-05
SOM	0.14446E-01	0.50905E-02	–0.41022E-02	0.36941E-04
10^7 Diff (%)	–0.01	–0.08	–0.12	- - -

Table 1c: Comparison of Stokes Vector Calculations

Flat Ocean Surface; View 3

	! I	Q	U	V
FMC	0.23151E+00	-0.18589E+00	-0.46336E-05	0.89707E-07
SOM	0.23519E+00	–0.18908E+00	0.0	0.0
10^7 Diff (%)	–1.56	–1.69	———	———

Table 2a: Comparison of Stokes Vector Calculations

Rough Ocean Surface; No Direct Sun Glitter; View 1

	I	Q	U	V
FMC	0.11631E-01	−0.46800E-02	−0.13808E-05	0.29246E-06
SOM	0.11654E-01	−0.46907E-02	−0.83606E-09	0.67416E-12
10^7 Diff (%)	−0.20	−0.23	– – –	– – –
10^8 Diff (%)	−0.10	−0.19	– – –	– – –

Table 2b: Comparison of Stokes Vector Calculations

Rough Ocean Surface; No Direct Sun Glitter; View 2

	I	Q	U	V
FMC	0.14439E-01	0.50779E-02	−0.41288E-02	−.85647E-05
SOM	0.14461E-01	0.50948E-02	−0.41417E-02	−.53699E-05
10^7 Diff (%)	−0.15	−0.33	−0.31	– – –
10^8 Diff (%)	−0.04	−0.15	−0.12	– – –

Table 2c: Comparison of Stokes Vector Calculations

Rough Ocean Surface; No Direct Sun Glitter; View 3

	I	Q	U	V
FMC	0.64462E-01	−0.29315E-01	−0.29313E-05	−.22861E-06
SOM	0.64610E-01	−0.29438E-01	−0.99255E-09	0.46572E-10
10^7 Diff (%)	−0.23	−0.42	– – –	– – –
10^8 Diff (%)	−0.16	−0.33	– – –	– – –

the atmosphere and the sea surface is identical to that used in preparation of the lookup tables; however, the computed test radiances will include the influence of the polarization induced by scattering from the atmosphere and reflection from the surface. We start be examining a situation in which the test model of the aerosol is one of the candidate aerosol models. In this case, were scalar radiative transfer theory the correct physics, and were the implementation of the algorithm

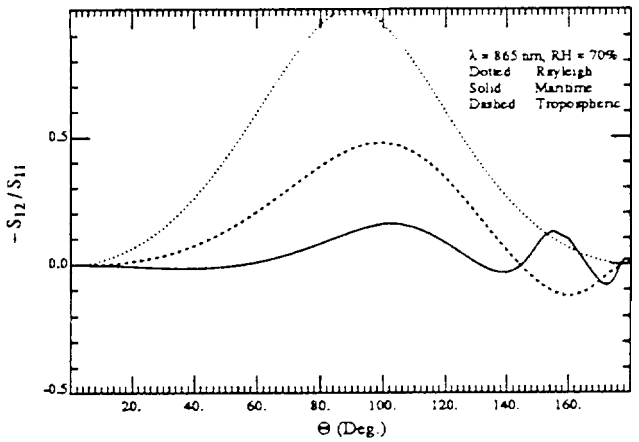

Figure 2a.

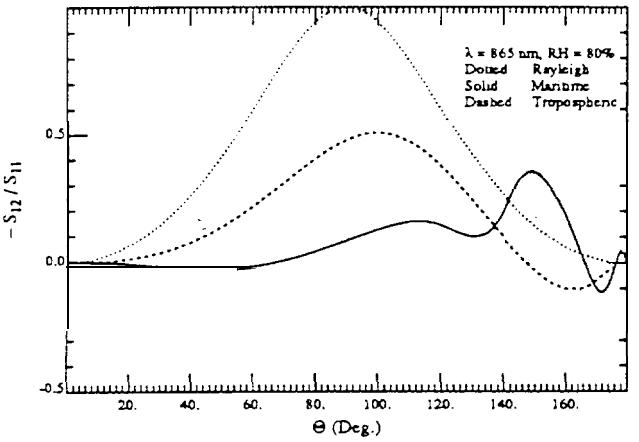

Figure 2b.

Figure 2. Degree of polarization of Rayleigh scattering and scattering by aerosols modeled as Maritime and Tropospheric: (a) RH = 70%; and (b) RH = 90%.

(see ATBD) exact, application of the correction algorithm to the test pseudo data generated by the Monte Carlo code operating in the scalar mode should yield a perfect atmospheric correction. The difference between application of the algorithm to test pseudo data generated by the Monte Carlo code operating in the scalar mode and operating in the full vector mode provides the polarization error in the algorithm under the most ideal conditions.

The degree of polarization of scattering for the test models used in this analysis is compared with that for molecular scattering (Rayleigh) at 865 nm in Figure 2. Figure 2a is for the Shettle and Fenn[6] Maritime and Tropospheric test models with a relative humidity (RH) of 70%. These

are actually members of the set of candidate aerosol models used in the algorithm. In contrast, Figure 2b is for models with with RH = 80%. These models are not members of the candidate set, therefore, they provide a more realistic test of the performance of the algorithm, and they were used for this purpose by Gordon and Wang.[7] Note that both the Tropospheric and Maritime models display considerably different polarization properties, and are both significantly different from Rayleigh scattering. Note also, that the degree of polarization of the Maritime model at RH = 80% is considerably different from that at RH = 70% in the important backscattering directions, 120°–1800.

The computations of the radiance leaving the top of the atmosphere are carried out for seven sun-viewing geometries: $\theta = 0$ with $\theta_0 = 20°$, 40°, and 60°, corresponding to viewing near the center of the MODIS scan; and $\theta = 45°$ and $\phi = 90°$ with $\theta_0 = 0$, 20°, 40°, and 60°, corresponding to viewing near the edge of the MODIS scan. Figure 3 provides $\Delta\rho$, the error in the water-leaving radiance at 443 nm after application of the correction algorithm to the simulations, as a function of the solar zenith angle, using the Maritime aerosol model at 70% RH for aerosol optical thicknesses of 0.2 and 0.4 at 865 nm. Recall that the first step in atmospheric correction is computation and removal of the radiance produced by Rayleigh scattering. In testing the algorithm throughout its development, the Rayleigh contribution was computed using scalar theory as was the ocean-atmosphere radiance. However, it is well known that ignoring polarization can cause significant errors in the Rayleigh contribution,[8] and in CZCS processing this contribution was determined using vector radiative transfer theory. [8] Thus, we expect that when using test pseudo data generated by a code using vector theory (or when applying the algorithm to actual MODIS imagery) it will be necessary to compute the Rayleigh contribution using vector theory. In contrast, when test pseudo data is generated using scalar theory, scalar theory must also be used to compute the Rayleigh contribution. Because of this, on each panel of the figure there are the results of three different applications of the algorithm. The fist is the “S-S” case in which the results of a scalar computation of the total radiance are used as test pseudo data, and the Rayleigh contribution is also computed using scalar theory. This corresponds to the situation under which the algorithm was developed, and in the absence of statistical fluctuations in the Monte Carlo simulations and inaccuracies in the implementation of the correction algorithm, $\Delta\rho$ should be negligible. The second is the “V-S”

case in which the top-of-atmosphere radiance is computed using vector theory but the Rayleigh contribution is computed using scalar theory. This would represent what on would expect if the algorithm were applied to MODIS imagery using a scalar computation of the Rayleigh contribution. In the final application of the algorithm, "V-V", the test pseudo data is computed using vector theory, as is the Rayleigh contribution. This simulates using the algorithm with MODIS imagery and correctly computing the Rayleigh contribution with vector theory.

The results presented in Figure 3 suggest that the implementation of the correction algorithm is excellent (S–S errors are $\leq$ 0.0008 and often much less even for $\tau_a(865)$ = 0.4). Furthermore, they show that when applying the algorithm to MODIS imagery the Rayleigh contribution must be computed using vector theory (V-S error is very large). Finally, the difference between the S–S and V–V results suggest that the errors caused by generating the atmospheric correction lookup tables using scalar theory are not excessive, although they are seen to increase with increasing $\tau_a(865)$, i.e., as aerosol scattering (and therefore polarization) becomes increasingly more important compared to Rayleigh scattering.

Similarly Figures 4 and 5 provide the comparison of the error in the water leaving radiance for the Maritime and Tropospheric aerosol models with RH = 80%. Recall that these models are *not* members of the candidate aerosol models and therefore one would expect larger errors than seen in Figure 3. For the Maritime case (Figure 4) the overall accuracy is similar to that in Figure 3; however, for the Tropospheric case (Figure 5) the error becomes excessive for $\tau_a(865)$ = 0.4 for both the S-S and V-V algorithms. This breakdown of the algorithm is caused by the large aerosol optical depth a 443 run (~ 1) which is actually outside the range of the computations used to prepare the lookup tables (i.e., requires extrapolation as opposed to interpolation in the lookup tables). However, the difference between the S–S and V-V algorithms is approximately independent of the optical depth which implies that the polarization effects are only a weak function of τ_a. The differences between the S–S and V-V algorithms for the results provided in Figures 3–5 show some consistent similarities. For example, in all of the cases at the scan edge the V–V results are lower than the S–S for $\theta_0 < 40°$ and higher for $\theta_0 > 40°$, with essentially no difference at $\theta_0 = 40°$. In contrast, for viewing near the scan center the V-V results are consistently lower than the S–S.

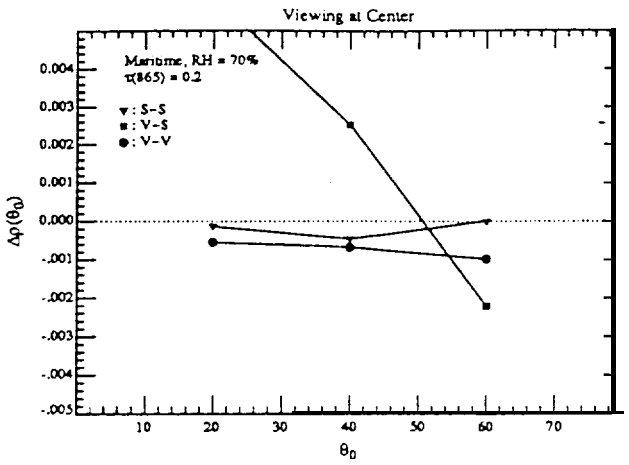

Figure 3a.

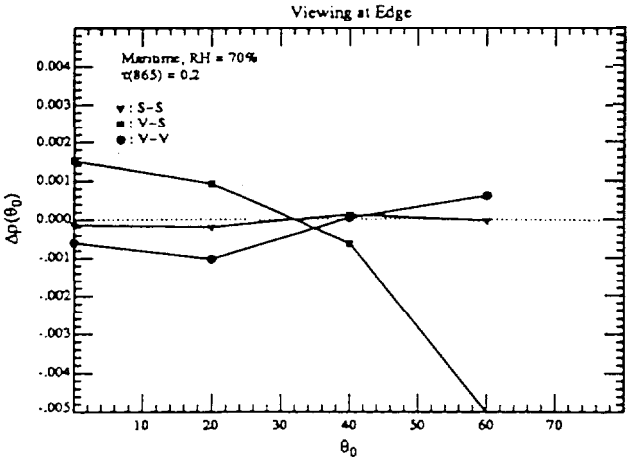

Figure 3b.

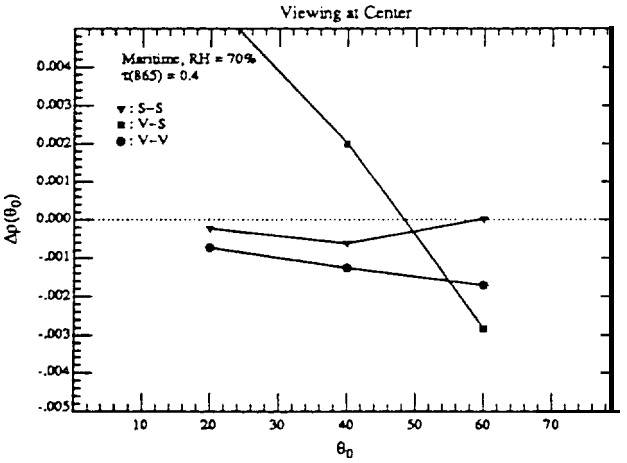

Figure3c.

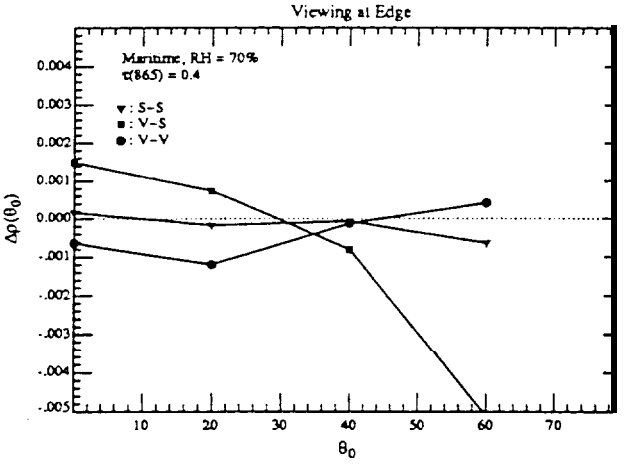

Figure 3d.

Figure 3. Error in the the water-leaving reflectance at 443 nm for the Maritime aerosol model with RH = 70%: (a) scan center with $\tau_a(865)$ = 0.2 and $\tau_a(443)$ = 0.2614; (b) scan edge with $\tau_a(865)$= 0.2 and $\tau_a(443)$= 0.2614; (c) scan center with $\tau_a(865)$ = 0.4 and $\tau_a(443)$ = 0.5228; and (d) scan edge with $\tau_a(865)$ = 0.4 and $\tau_a(443)$ = 0.5228.

It is noteworthy that the differences between V-V and S-S for the Maritime model with RH = 70% and $\tau_a(865)$ = 0.4 (Figures 3c and 3d) and the Tropospheric model with RH = 80% and $\tau_a(865)$ = 0.2 (Figures 5a and 5b) are practically identical. Both of these cases have $\tau_a(443)$ = 0.5 but the polarization properties of the aerosol 'models are completely different: the Tropospheric model being much closer to Rayleigh scattering than the Maritime model (Figure 2).

Thus far this study yields two important conclusions: (1) that most of the error due to the neglect of polarization can be removed by computing the Rayleigh contribution to the total reflectance using vector theory; and (2) the residual error due to the neglect of polarization in constructing the lookup tables is usually ~ 0.001 and appears to vary in a systematic manner with viewing geometry.

(iv) No work was performed on this task during this reporting period.

(v) No work was performed on this task during this reporting period.

c. Data/ Analysis/Interpretation: See item b above.

d. Anticipated Future Actions:

(i) We will continue our analysis of the existing simulations from the three-layer code to try to understand why the thin cirrus cloud simulations appear to yield anomalous results (See Appendix 1).

(ii) None. This task is now complete.

(iii) We will continue work on the effect of polarization on atmospheric correction.

(iv) We will begin this study using the Monte Carlo code developed under task (ii).

(iv) We will begin this study using the Monte Carlo code developed under task (ii).

e. Problems/Corrective Actions:

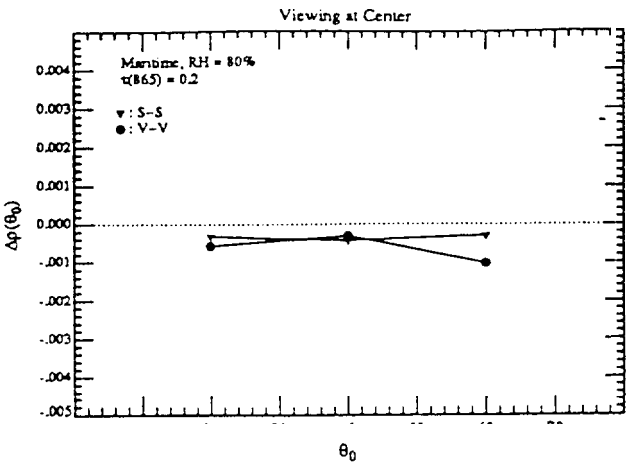

Figure 4a.

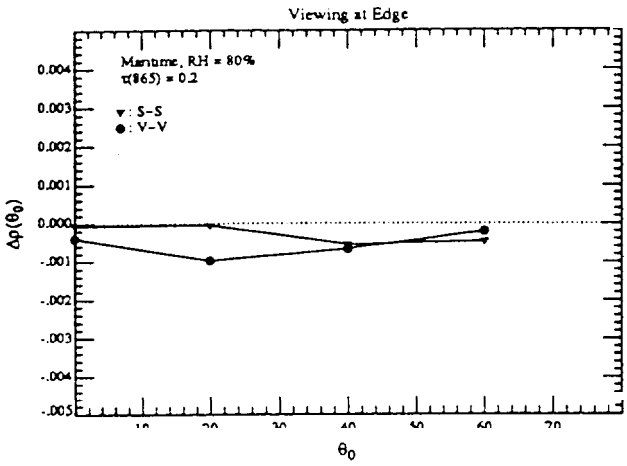

Figure 4b.

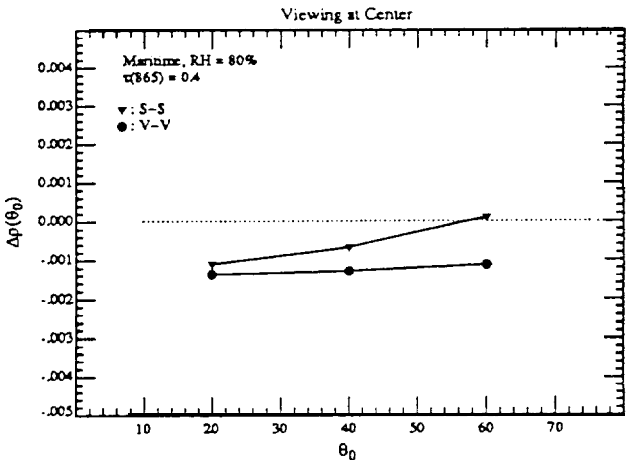

Figure 4c.

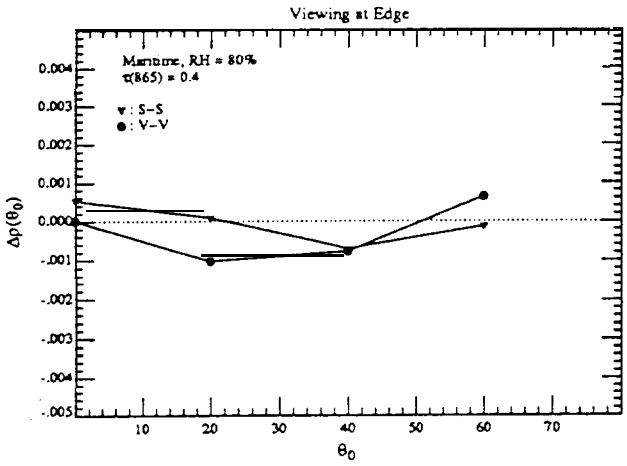

Figure 4d.

Figure 4. Error in the the water-leaving reflectance at 443 nm for the Maritime aerosol model with RH = 80%: (a) scan center with $T_a(865)$ = 0.2 and $T_a(443)$ = 0.2311; (b) scan edge with $T_a(865)$= 0.2 and $T_a(443)$ = 0.2311; (c) scan center with $T_a(865)$ = 0.4 and $T_a(443)$ = 0.4621; and (d) scan edge with $T_a(865)$ = 0.4 and $T_a(443)$ = 0.4621.

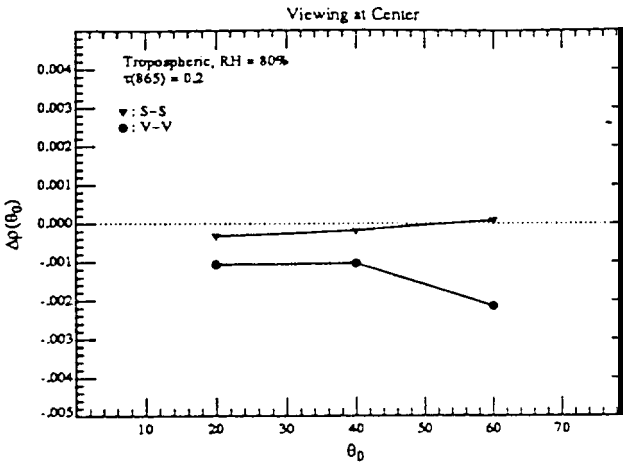

Figure 5a.

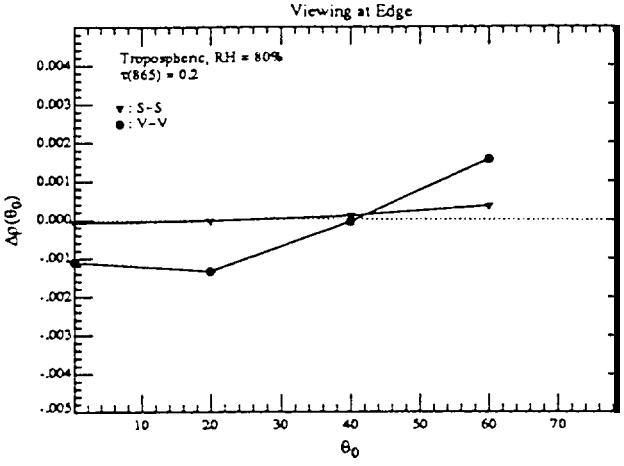

Figure 5b.

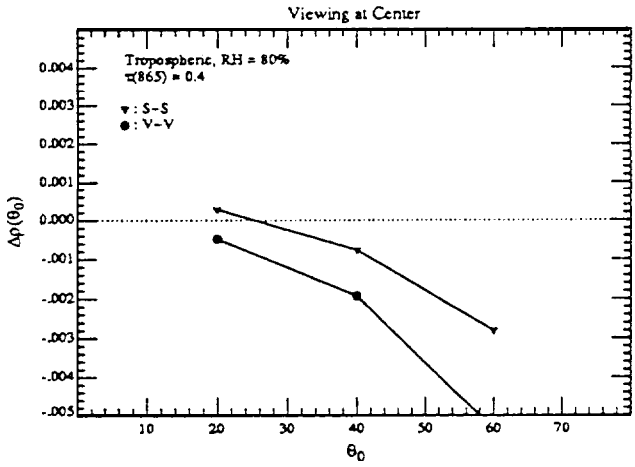

Figure 5c.

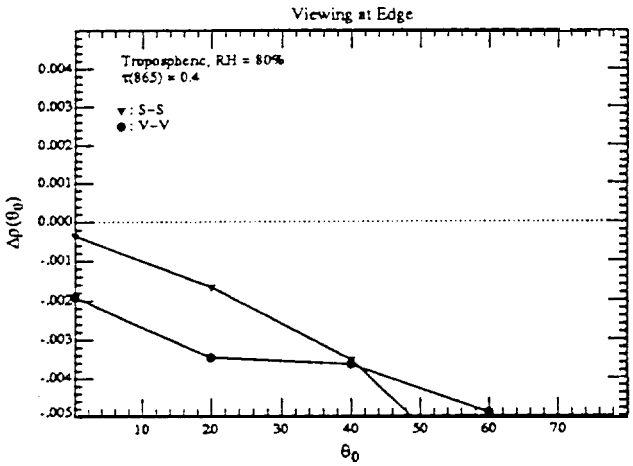

Figure 5d.

Figure 5. Error in the the water-leaving reflectance at 443 nm for the Tropospheric aerosol model with RH = 80%: (a) scan center with $T_a(865)$ = 0.2 and $T_a(443)$ = 0.4966; (b) scan edge with $T_a(865)$ =0.2 and $T_a(443)$ = 0.4966; (c) scan center with $T_a(865)$ = 0.4 and $T_a(443)$ = 0.9933; and (d) scan edge with $T_a(865)$ = 0.4 and $T_a(443)$ = 0.9933.

(i) None.

(ii) None.

(iii) None.

(iv) None.

(v) None.

f. Publications:

K. Ding and H.R. Gordon, Analysis of the influence of O_2 "A"-band absorption on atmospheric correction of ocean color imagery, *Applied Optics* 34, 2068–2080 (1995).

2. Whitecap Correction Algorithm

a. Task Objectives:

As we have described earlier, we have constructed and tested a whitecap radiometer for development and validation of the whitecap correction algorithm. It was first deployed during the last quarter of 1994. During the deployment we noted several aspects which needed improvement, thus our near term objectives were:

(i) adding a video system to the whitecap radiometer to allow us to understand the radiometer signal and pick out artifacts more accurately,

(ii) rebuilding the 5 channel deck cell (which measures the downwelling irradiance) to increase stability and reliability (also, we would increase the number of channels to 6 to match the upwelling radiance channels of the whitecap radiometers),

(iii) integrating a meteorology package into the whitecap radiometer system,

(iv) reducing and investigating the data obtained during October and November during the Hawaii MOCE-3 cruise, and

(v) participating in a cruise with Dennis Clark during June-July off the coast of Hawaii.

b. Work Accomplished:

We have selected the video system and procured it. We are using a Sony color security camera (SSC-C350), with a HI-8 video recorder (Sony EVC100), and an in-line time/date generator. This will allow us to obtain camera images, with a time date stamp which will allow us to match the data and video images. .4 housing for this camera is being built, and we expect to have this completed by mid-July.

We have all of the supplies needed for rebuilding the deck cell and we have the meteorology package in house. Both of these items will be fished by mid-July.

The cruise off of Hawaii during June-July was canceled so we could not participate.

c. Data/ Analysis/Interpretation:

We have performed some preliminary data reduction of the cruise data, but do not have any conclusions from this work at this point. The basic result thus far has been the requirement for simultaneous video imagery to enable the removal of artifacts. We are continuing analysis of the small quantity of data obtained during the few instances we were able to borrow a video camera from Dennis Clark, in order to develop a procedure for data analysis.

d. Anticipated Future Actions:

We are planning to participate in a short cruise at the end of July out of Ft. Pierce, FL. This will give us a chance to try out our latest modifications locally, and to obtain data in a different locale. We are also planning on participating on field tests with Dennis Clark in Hawaii, when these are scheduled. Presently we anticipate a field test in September in Hawaii during which we

will deploy the complete system. Due to the problems with the SeaWiFS launch, many of the other cruises we anticipated have been delayed, but we will try to find cruises-of-opportunity on which to field this instrument. Because this instrument does not make specific requirements on the ship operations, we believe we will be able to find many opportunities to “piggy-back” on other expeditions.

e. Problems/Corrective Actions: None.

f. Publications: None.

3. In-water Radiance Distribution.

a. Task Objectives:

Acquire radiance data at sea.

b. Work Accomplished: None

c. Data/ Analysis/Interpretation: None.

d. Anticipated Future Actions:

Acquire data at sea at the earliest opportunity. This will most Likely be a cruise scheduled by Dennis Clark in the Fall.

e. Problems/Corrective Actions: None.

f. Publications: None.

4. Residual Instrument Polarization.

a. Task Objectives: None.

5. Direct Sun Glint Correction.

a. Task Objectives: None.

6. Prelaunch Atmospheric Correction Validation.

a. Task Objectives:

The long-term objectives of this task are two-fold. First, we need to study the aerosol phase function and its spectral variation in order to verify the applicability of the aerosol models used in the atmospheric correction algorithm. Effecting this requires obtaining long-term time series of the aerosol optical properties in typical maritime environments. This will be achieved using a CIMEL sun/sky radiometer that can be operated in a remote environment and send data back to the laboratory via a satellite link. These are similar to the radiometers used by B. Holben and Y. Kaufman. Second, we must be able to measure the aerosol optical properties from a ship during initialization /calibration/validation cruises. The CIMEL-type instrumentation cannot be used (due to the motion of the ship) for this purpose. The required instrumentation consists of an all-sky camera (which can measure the entire sky radiance, with the exception of the solar aureole region, from a moving ship), an aureole camera (specifically designed for ship use), and a hand-held sun photometer. We have a suitable sky camera and sun photometer and must construct an aureole camera. Our objective for this calendar year is (1) to assemble, characterize and calibrate the solar aureole camera system, (2) to develop data acquisition software, and (3) to test the system. A second objective is to acquire a CIMEL Automatic Sun Tracking Photometer, calibrate it, and deploy it in a suitable location for studying the optical properties of aerosols over the oceans.

b. Work Accomplished:

We have the solar aureole camera system assembled along with a trial version of the data acquisition software. We have taken some test images, and are working to optimize the system performance. We had hoped to field this instrument during the cruise this summer; however as

mentioned in Section 2.b, it was canceled. We will deploy the instrument in some manner during the fall to obtain aureole data.

We have received the CIMEL instrument, and Dr. Brent Holben (NASA/GFSC) has performed a comparison calibration with his instruments, which have been calibrated at Mauna Loa, HI. We are presently installing the instrument at RSMAS, on Virginia Key in Miami for a short field test. During May we visited a site in the Dry Tortugas, a small set of islands in the Gulf of Mexico off of Key West. The main island is Fort Jefferson, part of the National Park Service. We found two sites at Ft. Jefferson which would be ideal for installation of the CIMEL instrument. This location has little ground reflectance problems, particularly in the infra-red, should provide a maritime atmosphere, and is conveniently close to Miami. As well as providing an excellent location for studying the properties of aerosols over the oceans, we believe it could also serve as an ideal site for MODIS vicarious calibration exercises. After visiting the site, a proposal to locate the CIMEL there was written and forwarded to the park service at Everglades National Park. We are now waiting for a response to this proposal, and given a positive response from the park service and a successful trial at RSMAS, we hope to install the instrument during the next reporting period.

c. Data/ Analysis/Interpretation: None

d. Anticipated Future Actions:

We will be acquiring data with the aureole camera system, in conjunction with the sky radiance distribution camera system sometime during this next reporting period. We will finish testing the CIMEL locally and by the end of the next period we will have the CIMEL instrument in place in a suitable location such as the Dry Tortugas.

e. Problems/Corrective Actions: None

f. Publications: None.

7. Detached Coccolith Algorithm and Post Launch Studies.

a. Task Objectives:

The algorithm for retrieval of the detached coccolith concentration from the coccolithophorid, E. huxleyi is described in detail in our ATBD. The key is quantification of the backscattering coefficient of the detached coccoliths. Our earlier studies showed that calcite-specific backscatter coefficient was less variable than coccolith-specific backscatter coefficient, and this would be more scientifically meaningful for future science that will be performed with this algorithm. The variance of the calcite-specific backscatter has been analyzed for only a few species, thus, we need to examine this in other laboratory cultures and field samples. There is also a relationship between the rate of growth of the calcifying algae and the rate of production and detachment of the coccoliths which needs to be further quantified. With this in mind, the objectives of our coccolith studies are, under conditions of controlled growth of coccolithophores (using chemostats), to define the effect of growth rate on:

- the rate that coccoliths detach from cells (which also is a function of turbulence and physical shear);
- the rates of coccolith production;
- the morphology of coccoliths; and
- the volume scattering and backscatter of coccoliths.

The last aspect of these studies will be to perform shipboard measurements of suspended calcite and estimate its optical backscatter as validation of the laboratory measurements. A thorough understanding of these growth-related properties will provide the basis for a generic suspended calcite algorithm. As with algorithms for chlorophyll, and primary productivity, the natural variance between growth related parameters and optical properties needs to be understood before the accuracy of the algorithm can be determined,

b. Work Accomplished:

Our controlled growth experiments with Emiliania huxleyi terminated dining the first week of May. Four growth rates were sampled at steady state, with replication.

c. Data/Analysis/Interpretation: Nothing additional since the last report.

d. Anticipated Future Actions:

All of the data obtained for volume scatter needs to be converted to backscatter values. Moreover, suspended calcite samples that were taken during the experiment need to be analyzed. We are currently switching our atomic absorption measurements to a new Perkin Elmer instrument at the University of Maine. This instrument has a graphite furnace attachment and will give us orders of magnitude more sensitivity. We are currently being trained on its use, and will begin running samples shortly. After the backscatter and calcite samples have been processed, we will proceed to calculate the calcite-specific backscatter coefficients as a function of growth rate (which is the ultimate goal of this experiment). Scanning electron micrographs will also be processed during the next two quarters to examine changes in coccolith morphology as a function of growth rate.

e. Problems/Corrective Actions: None

f. Publications:

Two papers were presented at the "Emiliania huxleyi and the Oceanic Carbon Cycle" meeting in London in April. the abstracts are provided below.

Calcification and Photosynthetic Rates of Coccolithophores Under Steady State Growth

W.M. Balch and J.J. Ritz

Rosenstiel School for Marine and Atmospheric Science

University of Miami

4600 Rickenbacker Causeway

Miami, FL 33155

Carbon fixation of Emiliania huxleyi was studied in light limited, steady state, continuous cultures. Six growth rates were examined ranging from $0.24d^{-1}$ to $1.0d^{-1}$ although the lowest may have been carbon limited and the highest approached washout. Both photosynthesis and calcification increased as a function of growth rate, but the ratio of calcification to photosynthesis (C/P) was not constant; that is, C/P increased from about 0.2 to 0.7 as the growth rate increased from $0.24d^{-1}$ and $0.75d^{-1}$, then the ratio decreased slightly at higher growth rates. Extrapolation of the regression data suggested that there should be zero calcification at a growth rate of about $0.15d^{-1}$. Cells were also given a 30s acidification/neutralization treatment to dissolve their coccoliths, and then carbon fixation was measured. Photosynthesis and calcification increased by about 0.1 pg C $cell^{-1}$ h^{-1} following this treatment. Total carbon fixation rate was predicted by multiplying the total carbon per unit chlorophyll by the respective culture dilution rate. These predictions were almost identical to total carbon incorporation measured using 14C bicarbonate. Nevertheless, to accurately predict only photosynthesis or calcification using this approach also will require the function relating the C/P ratio to growth rate.

A coccolith detachment rate determined from chemostat cultures of the coccolithophore Emiliania huxleyi

J.J. Ritz and W.M. Balch

Rosenstiel School for Marine and Atmospheric Science

University of Miami

4600 Rickenbacker Causeway

Miami, FL 33155

The coccolithophore Emiliania huxleyi (Lohm.) Hay and Mohler is one of the most abundant calcite producing organisms on earth and consequently, the coccoliths represent a major carbon sink in the ocean. This study addresses the rate of detachment of coccoliths from the coccolithophores under controlled growth conditions using light-limited chemostats. Cultures were grown at six different growth rates between 0.24 day^{-1} and 1.00 day^{-1}. Other cell properties including chlorophyll, particulate inorganic carbon, and total particulate carbon, were also investigated with

regard to the growth rate of the cells. The coccolith detachment rate increased linearly with cellular growth rate at almost a 1:1 ratio. Such a change in detachment with growth could affect several processes such as sinking rates of cells and bloom formation. The discussion ends with a section on the importance of sinking to coccolithophores.

8. Other Developments.

The PI participated the MOCEAN Team meeting and the Multisensor Calibration and Validation Workshop in Miami in February 1995. Also, the PI prepared a first draft of a validation plan for normalized water-leaving radiance and forwarded it to Frank Hoge and Wayne Esaias for incorporation into the MODIS Ocean Products Validation Plan. This draft is included here as an appendix. A shortened version was prepared for the report of the Multi sensor Calibration and Validation Workshop to be submitted to NASA Headquarters.

In May, the PI attended the CEOS/IVOS Calibration and Validation Workshop and presented a review, *Theoretical Basis of the SeaWiFS/MODIS Normalized Water-leaving Radiance Algorithm (Atmospheric Correction) and its relationship to Vicarious Calibration.*

A method for combining high-altitude aircraft radiance (upwelling) and surface radiance (downwelling) for determination of the columnar aerosol optical properties has been developed. A paper on the subject,

H.R. Gordon and T. Zhang, Columnar Aerosol Properties Over Oceans
by Combining Surface and Aircraft Measurements: Simulations.

was accepted for publication and is now in press in *Applied Optics.* This work could provide a powerful method of studying aerosol properties over the ocean. This paper is attached as Appendix 2. A second study concerning the perturbation of the sky radiance measurements made from islands, caused by the presence of the island itself, has been carried out and a paper

H. Yang, H.R. Gordon and T. Zhang, Island perturbation to the sky radiance over the ocean: Simulations,

was submitted to *Applied Optics.* The paper completed the fist review and is now under revision. It is attached as Appendix 3. Both of these have relevance to the "Prelaunch Atmospheric Correction Validation" (Topic 6 above) portion of our research, as well as to the validation of retrieved aerosol properties over the oceans from EOS sensors.

A method for dealing with out-of-band response of ocean color sensors was developed by the PI. A paper

H.R. Gordon, Remote sensing of ocean color: a methodology for dealing with broad spectral bands and significant out-of-band response,

was prepared and submitted to *Applied Optics.* This work is applicable to any ocean color sensor, and the same methodology will be employed for MODIS. It is attached here as Appendix 4.

9. References.

[1] H. R. Gordon and M. Wang, "Surface Roughness Considerations for Atmospheric Correction of Ocean Color Sensors. 1: The Rayleigh Scattering Component," Applied Optics 31, 4247–4260 (1992).

[2] H. C. van de Hulst, *Multiple Light Scattering* (Academic Press, New York, 1980), 739 pp.

[3] H. R. Gordon and M. Wang, "Surface Roughness Considerations for Atmospheric Correction of Ocean Color Sensors. 2: Error in the Retrieved Water-leaving Radiance, " Applied Optics 31, 4261-4267 (1992).

[4] H. Quenzel and M. Kastner, "optical properties of the atmosphere: calculated variability and application to satellite remote sensing of phytoplankton, " Applied Optics 19, 1338–1344 (1980).

[5] C. Cox and W. Munk, "Measurements of the Roughness of the Sea Surface from Photographs of the Sun's Glitter," Jour. Opt. Sot. of Am. 44, 838-850 (1954).

[6] E. P. Shettle and R. W. Fenn, *Models for the Aerosols of the Lower Atmosphere and the Effects of Humidity Variations on Their Optical Properties* (Air Force Geophysics Laboratory, Hanscomb AFB, MA 01731, AFGL-TR-79-0214, 1979).

[7] H. R. Gordon and M. Wang, "Retrieval of water-leaving radiance and aerosol optical thickness over the oceans with SeaWiFS: A preliminary algorithm," Applied Optics 33,443-452 (1994).

[8] G. W. Kattawar, G. N. Plass and S. J. Hitzfelder, "Multiple scattered radiation emerging from Rayleigh and continental haze layers. 1: Radiance, polarization, and neutral points," Applied Optics 15, 632-647 (1976).

[9] H. R. Gordon, J. W. Brown and R. H. Evans, "Exact Rayleigh Scattering Calculations for use with the Nimbus-7 Coastal Zone Color Scanner," Applied Optics 27, 862-871 (1988).